View Article Online
View Journal

Organic & Biomolecular Chemistry

Accepted Manuscript

This article can be cited before page numbers have been issued, to do this please use: J. Gao, X. Yin, M. Li, J. Chen, J. Tan, Z. Zhao and X. Gu, *Org. Biomol. Chem.*, 2020, DOI: 10.1039/D0OB00082E.

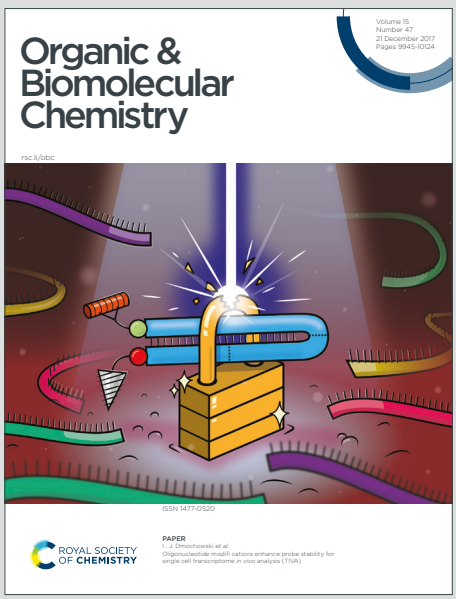

ROYAL SOCIETY OF CHEMISTRY

rsc.li/obc

View Article Online
DOI: 10.1039/D0OB00082E

COMMUNICATION

Rational Design of Fluorescent Probes for Targeted *in vivo* Nitroreductase Visualization

Received 00th January 20xx,
Accepted 00th January 20xx

DOI: 10.1039/x0xx00000x

Jie Gao[a$], Xiaofan Yin [a$], Mimi Li[a], Ji-An Chen[a], Jiahui Tan[a], Zhen Zhao [a*], Xianfeng Gu[a*]

Nitroreductase (NTR) has been recognized as a biomarker for identifying the hypoxic status of cancers. Therefore, it is of high scientific interest to design effective fluorescent probes for tracking NTR activity. However, studies are rarely reported to disentangle the structure–performance relationship of fluorescent probes and provide valuable insight into optimized probe design. Three BODIPY based fluorescent probes were made by conjugation of para-, ortho-, and meta-nitrobenzene to BODIPY core via thiolether bond, respectively. Our study revealed that the linkage and nitro substituent position significantly influence the capability of Nitroreductase detection.

Tumor hypoxic microenvironments are caused by abnormal angiogenesis and rapacious demands of oxygen by fast dividing cancer cells. Hypoxia microenvironments are usually observed in most of solid tumors where the median oxygen concentration has been reported to be around 4-0 % locally, adapted and exploited by cancer cells for their survival and invasion.[1] The worst thing about tumor hypoxic microenvironments is that it has been regarded as one of the major causes of the resistance to various therapies including immunotherapy.[2] Therefore, estimating the tumor issue and cells hypoxia degree is of great importance in predicting anticancer efficacies.

In tumor hypoxic microenvironments, tumor cells display enhanced endogenous nitroreductase (NTR) activities, enabling NTR an attractive target for selectively and efficiently measuring hypoxia in tumor cells or tumor tissue.[3] NTR is flavoenzymes that catalyze the reduction of a variety of nitroaromatic compounds using NAD(P)H as source of reducing equivalents.[4] To date, several imaging techniques have been developed, such as NMR,[5] PET[6] and fluorescence[3e, 4b, 7] to monitoring NTR activities in biological system based on the changes of physical and chemical properties caused by the NTR-catalysed reduction of the nitro group in substrate into an amino group. Particularly, fluorescence imaging is attractive on tracing the changes and activities of biological targets due to their exceptional sensitivity. Therefore, several fluorescent probes for detection of NTR activities *in vitro* and *in vivo* have been reported by employing a para-nitroaromatic group as reaction and recognition group.[4b, 7b, 8] For example, Li's group reported a series of NTR probes with a nitro group at para-, ortho-, and meta-phenyl position, respectively. It was found that only the probe with a para-nitrophenyl group via an ester linkage to fluorescent dye displayed significant fluorescent response to NTR.[7b] Despite these advancements, few studies have focused on the structure–performance relationship of fluorescent probes wherein the linkage between fluorophores and aromatic nitro group as well as nitro substituent position can dramatically induce the change of fluorescence, thus sensitively influencing the NTR activity assay.

To deeply disentangle such issues, we herein designed and synthesized three BODIPY based fluorescent probes (**BpS**, **BoS** and **BmS**) by conjugation of para-, ortho-, and meta-nitrobenzene to BODIPY core via thiolether bond, respectively. We expected that the nitro groups in the probes could be reduced into amino groups under the catalyzation of NTR, and the amino group resulting from **BoS** rather than from **BpS** or **BmS** would trigger an intramolecular nucleophilic substitution through five-membered cyclic transition state, finally yielding an amino substituted BODIPY. As sulfenyl-substituted BODIPYs showed markedly different optical properties from amino-substituted BODIPYs, thus detection of NTR activities could be achieved by monitoring fluorescence changes of **BoS**. As expectedly, these three probes showed different fluorescent responsiveness to NTR: **BpS** displayed a fluorescence turn off response to NTR; a weak turn on fluorescent signal was observed for **BmS**; and **BoS** exhibited a significant turn on fluorescent response to NTR. Due to the unique fluorescence light up, **BoS** was successfully used for the detection of NTR activities in living HeLa and HepG-2 cells under different hypoxic conditions. Importantly, **BoS** realized the selective identification of tumor hypoxia by real time monitoring of NTR activity *in vivo*.

[a.] *School of Pharmacy & Minhang Hospital, Fudan University, Shanghai 201301, China. E-mail :. xfgu@fudan.edu.cn； zhaozhen72@126.com.*

Electronic Supplementary Information (ESI) available: Procedures for synthesis, characterization data, and supplementary figures. See DOI: 10.1039/x0xx00000x

BpS, **BoS** and **BmS** were prepared via the aromatic substitution between the key intermediate **2** and para-, ortho-, and meta-nitrobenzene thiol (Scheme 1). Compound **2** was obtained via the condensation of compound **5** with compound **8**, followed by boron insertion with $BF_3{\cdot}Et_2O$ (Scheme 1 and S1).[9] para-, ortho-, and meta-nitrobenzene thiol **1** were synthesized from the reduction of the corresponding nitrophenyl disulfane (scheme 1). All the structures were fully characterized by ^{1}H NMR, ^{13}C NMR and HRMS (Figure S6-S11).

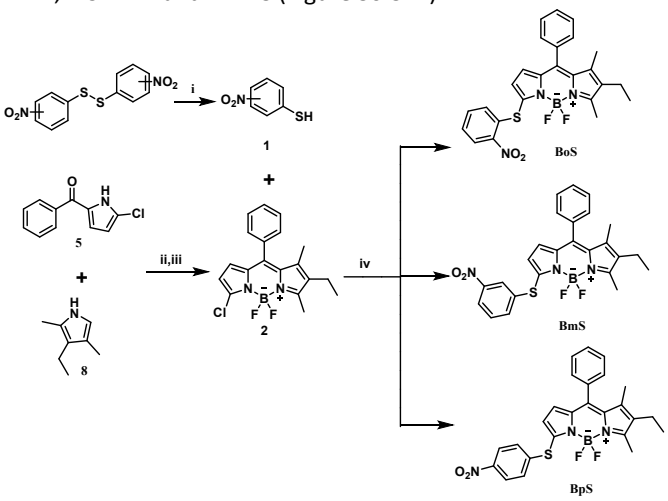

Scheme 1. The synthetic procedures of **BoS**, **BmS**, **BpS**. (i) $NaBH_4$, THF; (ii) $POCl_3$, CH_2Cl_2; (iii) Et_3N, $BF_3{\cdot}Et_2O$ (iv)) DMAP, MeCN.

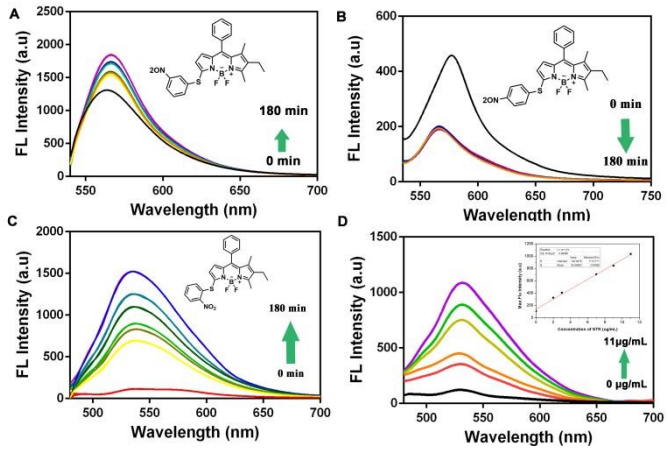

Figure 1. Time-dependent spectra changes of **BmS**, **BpS**, **BoS** (10 μM) in the presence of NTR (10 μg/mL) and NADH (0.5 mM) in buffer (MeCN/Tris-HCl, v/v, 1:3, pH 7.4) at 37 °C. (A) fluorescence spectral changes of **BmS** (λ_{ex} = 510 nm, λ_{em} = 565 nm), (B) fluorescence spectral changes of **BpS** (λ_{ex} = 510 nm, λ_{em} = 580 nm), (C) fluorescence spectral changes of **BoS** (λ_{ex} = 450 nm, λ_{em} = 540 nm). (D) The linear relationship between the fluorescence intensity of **BoS** (10 μM) at 540 nm and the concentrations of NTR (0-11 μg/mL) in the presence of NADH (0.5 mM, λ_{ex} = 450 nm). (D) The linear relationship between the fluorescence intensity of **BoS** (10 μM) at 540 nm and the concentrations of NTR (0-11 μg/mL) in the presence of NADH (0.5 mM, λex = 450 nm) for 180 min.

To evaluate the photophysical properties of **BpS**, **BmS** and **BoS** in the presence/absence of NTR and NADH, the absorption and fluorescence emission spectra of these three probes in Tris-HCl buffer (pH 7.4; 25 % MeCN) were investigated. Impressively, the three probes displayed different fluorescent responses to NTR. The addition of NTR to the solution of **BoS** resulted in an obvious fluorescence turn-on response with maximum emission at 540 nm when the excitation wavelength was 450 nm (Figure 1C), producing 13-fold increase. And the "turn on" effect by BOS can be supressed by the inhibitor of NTR which indicate the essential of NTR for activation the probe (Figure S3). However, NTR only triggered a weak fluorescent increase around 565 nm in the solution of **BmS** (Figure 1A). In contrast, upon addition of NTR in the solution of **BpS**, a significant fluorescence turn-off response around 580 nm was observed (Figure 1B). In view of the excellent fluorescence responsiveness of **BoS** to NTR, its linear fluorescent response NTR was further investigated. The kinetic profiles of **BoS** treated with the various concentrations of NTR were shown in Figure 1D. Notably, the fluorescence intensity increased linearly with concentrations of NTR increased from 0 to 11 μg/mL, contributing to a detection limit of 0.022 μg/mL (Figure 1D). These results indicate that **BoS** is a promising probe for detecting NTR under physiological conditions.

To understand the probes interactive behavior with nitroreductase, molecular docking simulations were performed to dock probes **BoS**, **BpS**, **BmS** into NTR (PDB code 4DN2) using the Glide module encoded in Schrodinger 3.5 software package, with Extra Precision (GlideXP) algorithm. Probe **BoS** tends to approach the hydrophobic interspace of NTR by the aromatic rings π-π interactions. Hydrogen bonds are also constructed between the O atom of **BoS** and the NTR amino acid residues. The probe forms five hydrogen bonds with NTR. Three is for the Arg 10 amino acid residues of NTR with the O atom of the nitro group of **BoS**, and the other two hydrogen bonds are for the Arg 172 residues with the O atom of the nitro group, which indicated the strong binding energy between **BoS** and NTR (Figure 2A). In contrast, although probes **BmS** and **BpS** can approach the hydrophobic interspace of NTR by the aromatic rings π-π interactions, only two hydrogen bonds were formed in **BmS**, **BpS** counterparts (Figure 2B and 2C).

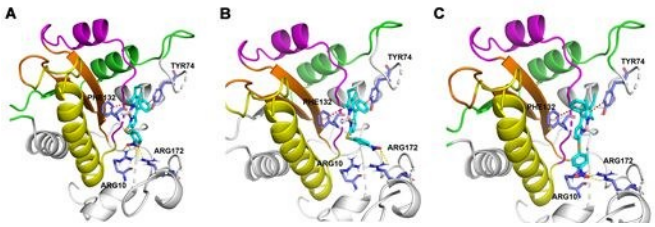

Figure 2. Calculated binding model of BoS (A), BmS (B), BpS (C) with NTR. The C, N and O atoms of probes structures are shown in blue, cyan and red, respectively. Hydrogen bonds are

indicated with yellow dotted lines, aromatic rings π-π interactions are indicated with red dotted lines.

The deduced detection mechanism of **BoS** activated by NTR was shown in Figure 3. The NTR catalysed reduction of nitro group into amino group initiated an intramolecular nucleophilic aromatic substitution (SNAr) via a five-membered cyclic transition state, which finally yield an amino substituted BODIPY with a free thiol group. As the sulfur-substituted and amino-substituted BODIPYs have the same molecular weight, it is difficult to identify the deduced detection mechanism by HRMS spectrometric analysis. Considering that there is a free thiol group in the amino substituted derivative, the thiol scavenger (N-methylmaleimide) was added in the reaction solution. The further HRMS spectrometric analysis indicated occurrence of the reaction between thiol and thiol scavenger, which confirmed our deduced mechanism (Figure 3).

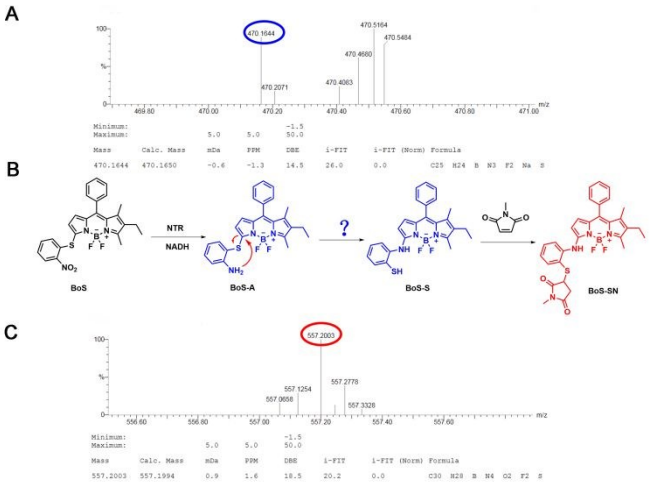

Figure 3. The deduced detection mechanism of **BoS** to NTR confirmed by HRMS. (A) Mass spectrum of reduced products (**BoS-A** or **BoS-S**), HRMS (ESI, m/z): calculated for $C_{25}H_{24}BF_2N_3S$ $[M+Na]^+$: 470.1650, found: 470.1644. (B) The deduced detection mechanism of **BoS** to Nitroreductase. (C) Mass spectrum of **BoS-SN**, HRMS (ESI, m/z): calculated for $C_{30}H_{29}BF_2N_4O_2S$ $[M-H]^-$:557.1994, found: 557.2003.

Before using **BoS** for its potential application in living cell imaging, the specificity and cytotoxicity of **BoS** have been explored. **BoS** exhibited high specificity towards NTR even in presence of bio thiols (Figure S2). And the cytotoxicity towards the HeLa and HepG-2 cells was determined by a CCK-8 assay (Figure S6). In the presence of **BoS** at 0–50 μM, the cellular viabilities were estimated to be >70 % after incubation for 24 hours. The results indicated that **BoS** has very low toxicity.
The capability of **BoS** for the intracellular NTR imaging was evaluated on hypoxia HeLa and HepG-2cells by confocal fluorescence microscopy. The HeLa and HepG-2 cells were cultured under normoxic conditions (20 % O_2) and hypoxic condition (1 % O_2) for 12 h and 24 h, and then treated with 10 μM **BoS** for 30 min. As shown in Figure 4, negligible fluorescence increases under the normoxic conditions were observed both in HeLa and HepG-2 cells. When the cells were cultured under the hypoxic conditions for 24 h, both HeLa and HepG-2 cells showed the great increase in the fluorescence intensity (Figure 4). In contrast, addition of dicoumarol, an NTR inhibitor, led to weaker emission in green channels. All these results indicated that the **BoS** can discriminate hypoxic tumor cells from normal cells based on the NTR expression levels. Costaining experiments were employed to identify the location of BoS utilizing commercially available Mito-Tracker Deep Red FM and Lyso-Tracker Deep Red (Figure S7). The overlapped fluorescence images of red fluorescence from Mito-Tracker Deep Red FM/ Lyso-Tracker Deep Red and NTR induced green fluorescence from BoS indicated that probe BoS possessed nonspecific intracellular localization.

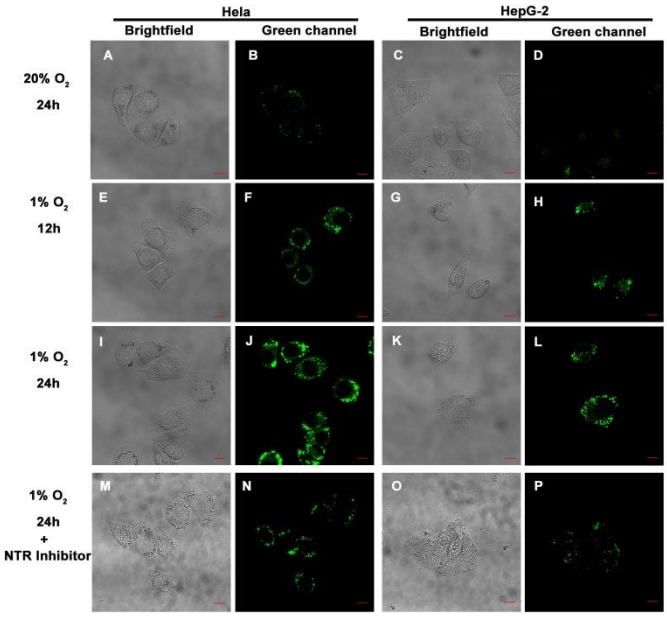

Figure 4. Confocal fluorescence images of living Hela and HepG-2 cells. (A-D) The Hela and HepG-2 cells were grown under normoxic condition (20 % O_2) for 24 h, and then incubated with 10 μM probe **BoS** for 30 min. (E-H) Hela and HepG-2 cells were grown under hypoxic condition (1 % O_2) for 12 h, and then incubated with 10 μM probe **BoS** for 30 min. (I-L) Hela and HepG-2 cells were grown under hypoxic condition (1 % O_2) for 24 h, and then incubated with 10 μM probe **BoS** for 30 min. (M-P) Hela and HepG-2 cells were grown under hypoxic condition (1 % O_2) for 24 h, and then incubated with 1 mM dicoumarol for 1 h, followed with probe **BoS** (10 μM) for 30 min. Green channel at 500-580 nm with λ_{ex} = 488 nm. The scale bar is 10 μm.

Encouraged by the results of living cell imaging, the capability of BoS as a fluorescent probe for animal bioimaging in vivo was further investigated. After direct injection of BoS (100 nmol) in Tris-HCl buffer into a HepG-2-tumor-bearing nude mice, images were recorded at various times by using IVIS spectrum imaging system. The tumor site displayed a significant enhancement fluorescence intensity within minutes. The signal eventually reached a plateau at 60 min post-injection. In contrast, there is no obvious fluorescence increasing in normal site after injection of BoS. The results demonstrated that the probe BoS is suitable to bioimaging hypoxic tumor in vivo (Figure 5).

View Article Online
DOI: 10.1039/D0OB00935E

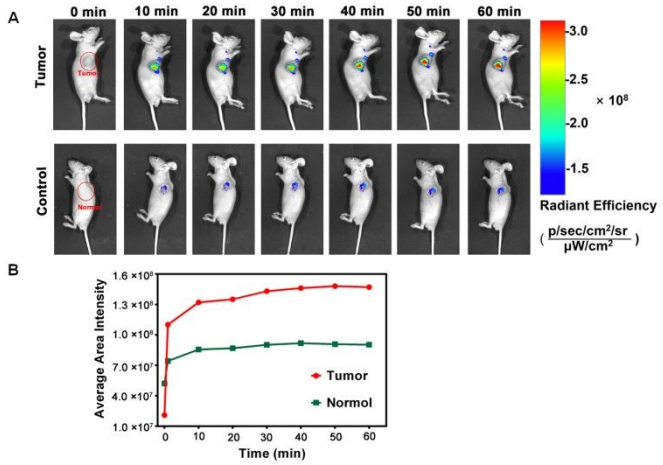

Figure 5. Time dependent *in vivo* fluorescence imaging of HepG-2 tumor-bearing mice model. (A) The time dependent fluorescence signals in tumor and normal sites of the tumor-bearing mice with injection of probe **BoS** (100 nmol) in Tris-HCl via intratumoral injection. (B) The fluorescence intensity changing of tumor (red) and normal injection sites (green). The fluorescence signals were collected between 560 nm-580 nm using λ_{ex} = 460 nm.

Conclusions

In summary, we have designed and synthesized a series of probes with para-nitrophenyl sulfide, meta-nitrophenyl sulfide and ortho-nitrophenyl sulfide respectively as recognition group for NTR detection. **BoS**, the probe with ortho-nitrophenyl sulfide displayed high sensitivity and excellent selectivity, with a distinct fluorescence off-on response to NTR. HRMS validated the occurrence of the sulfur-nitrogen translocation reaction. The efficient NTR detection ability of **BoS** was further validated by fluorescence imaging of hypoxic cells (Hela and HepG-2 cells) with overexpressed NTR. Importantly, **BoS** realized the selective identification of tumor hypoxia by real time monitoring of NTR activity *in vivo*. All the results demonstrate that ortho-nitrophenyl sulfide also can be the recognition group of the probe for detection of NTR.

Conflicts of interest

There are no conflicts to declare.

Notes and references

1 (a) M. Z. Noman, M. Hasmim, A. Lequeux, M. Xiao, C. Duhem, S. Chouaib, G. Berchem and B. Janji, *Cells*, 2019, **8**, 1083; (b) J. M. Brown and W. R. Wilson, *Nat. Rev. Cancer*, 2004, **4**, 437.

2 (a) A. R. Padhani, K. A. Krohn, J. S. Lewis and M. Alber, *Eur. Radiol.*, 2007, **17**, 861; (b) W. Meng, Y. Hao, C. He, L. Li and G. Zhu, *Mol. Cancer*, 2019, **18**, 57.

3 (a) J. Sun, Z. Hu, R. Wang, S. Zhang and X. Zhang, *Anal. Chem.*, 2019, **91**, 1384; (b) E. McCormack, E. Silden, R. M. West, T. Pavlin, D. R. Micklem, J. B. Lorens, B. E. Haug, M. E. Cooper and B. T. Gjertsen, *Cancer Res.*, 2013, **73**, 1276; (c) A. Chevalier, Y. Zhang, O. M. Khdour, J. B. Kaye and S. M. Hecht, *J. Am. Chem. Soc.*, 2016, **138**, 12009; (d) F. Xu, M. Fan, S. Kang and X. Duan, *Anal. Chim. Acta*, 2019, **1088**, 131; (e) Z. He, Y. Chou, H. Zhou, H. Zhang, T. Cheng and G. Liu, *Org. Biomol. Chem.*, 2018, **16**, 3266.

4 (a) Q. Su, P. A. Boucher and S. E. Rokita, *Angew. Chem. Int. Ed.*, 2017, **56**, 10862; (b) B. Huang, W. Chen, Y. Q. Kuang, W. Liu, X. J. Liu, L. J. Tang and J. H. Jiang, *Org. Biomol. Chem.*, 2017, **15**, 4383.

5 (a) D. Xie, T. L. King, A. Banerjee, V. Kohli and E. L. Que, *J. Am. Chem. Soc.*, 2016, **138**, 2937; (b) K. Tanabe, H. Harada, M. Narazaki, K. Tanaka, K. Inafuku, H. Komatsu, T. Ito, H. Yamada, Y. Chujo, T. Matsuda, M. Hiraoka and S. Nishimoto, *J. Am. Chem. Soc.*, 2009, **131**, 15982.

6 (a) Y. Shimizu, S. Zhao, H. Yasui, K. I. Nishijima, H. Matsumoto, T. Shiga, N. Tamaki, M. Ogawa and Y. Kuge, *Mol. Imaging Biol.*, 2019, **21**, 122; (b) L. Li, Y. Wei, Y. Huang, Q. Yu, W. Liu, S. Zhao, J. Zheng, H. Lu, J. Yu and S. Yuan, *Mol. Imaging Biol.*, 2018, **20**, 1061; (c) P. D. Bonnitcha, A. L. Vavere, J. S. Lewis and J. R. Dilworth, *J. Med. Chem.*, 2008, **51**, 2985; (d) E. Melsens, E. De Vlieghere, B. Descamps, C. Vanhove, K. Kersemans, F. De Vos, I. Goethals, B. Brans, O. De Wever, W. Ceelen and P. Pattyn, *Radiat. Oncol.*, 2018, **13**, 39.

7 (a) Y. Fang, W. Shi, Y. M. Hu, X. H. Li and H. M. Ma, *Chem. Commun.*, 2018, **54**, 5454; (b) Y. Li, Y. Sun, J. Li, Q. Su, W. Yuan, Y. Dai, C. Han, Q. Wang, W. Feng and F. Li, *J. Am. Chem. Soc.*, 2015, **137**, 6407; (c) Z. Thiel and P. Rivera-Fuentes, *Angew. Chem. Int. Ed.*, 2019, **58**, 11474; (d) R. Wang, J. Chen, J. Gao, J.-A. Chen, G. Xu, T. Zhu, X. Gu, Z. Guo, W.-H. Zhu and C. Zhao, *Chem. Sci.*, 2019, **10**, 7222; (e) Y. Liu, W. Liu, H. Li, W. Yan, X. Yang, D. Liu, S. Wang and J. Zhang, *Anal. Chim. Acta*, 2018, **1024**, 177.

8 (a) J. G. Bae, L. E. McNamara, M. A. Nael, F. Mahdi, R. J. Doerksen, G. L. Bidwell, N. I. Hammer and S. B. Jo, *Chem. Commun.*, 2015, **51**, 12787; (b) X. Tian, Z. Li, Y. Sun, P. Wang and H. Ma, *Anal. Chem.*, 2018, **90**, 13759; (c) S. Luo, R. Zou, J. Wu and M. P. Landry, *ACS Sens.*, 2017, **2**, 1139.

9 (a) C. Zhao, X. Zhang, K. Li, S. Zhu, Z. Guo, L. Zhang, F. Wang, Q. Fei, S. Luo, P. Shi, H. Tian and W. H. Zhu, *J. Am. Chem. Soc.*, 2015, **137**, 8490; (b) G. Xu, Q. Yan, X. Lv, Y. Zhu, K. Xin, B. Shi, R. Wang, J. Chen, W. Gao, P. Shi, C. Fan, C. Zhao and H. Tian, *Angew. Chem. Int. Ed.*, 2018, **57**, 3626.